The Radial Speed – Expansion Speed Relation for Earth-Directed CMEs

P. Mäkelä,[1,2] N. Gopalswamy,[2] and S. Yashiro[1,2]

[1]Department of Physics, The Catholic University of America, Washington, District of Columbia, USA.

[2]NASA Goddard Space Flight Center, Greenbelt, Maryland, USA.

Abstract. Earth-directed coronal mass ejections (CMEs) are the main drivers of major geomagnetic storms. Therefore, a good estimate of the disturbance arrival time at Earth is required for space weather predictions. The STEREO and SOHO spacecraft were viewing the Sun in near-quadrature during January 2010- September 2012, providing a unique opportunity to study the radial speed (V_{rad}) - expansion speed (V_{exp}) relationship of Earth-directed CMEs. This relationship is useful in estimating the V_{rad} of Earth-directed CMEs, when they are observed from Earth-view only. We selected 19 Earth-directed CMEs observed by the LASCO/C3 coronagraph on SOHO and the SECCHI/COR2 coronagraph on STEREO during January 2010-September 2012. We found that of the three tested geometric CME models the full ice-cream cone model of the CME describes best the V_{rad}-V_{exp} relationship, as suggested by earlier investigations. We also tested the prediction accuracy of the empirical shock arrival (ESA) model proposed by *Gopalswamy et al.* [2005a], while estimating the CME propagation speeds from the CME expansion speeds. If we use STEREO observations to estimate the CME width required to calculate the V_{rad} from the V_{exp} measurements, the mean absolute error (MAE) of the shock arrival times of the ESA model is 8.4 hours. If the LASCO measurements are used to estimate the CME width, the MAE still remains below 17 hours. Therefore by using the simple V_{rad}-V_{exp} relationship to estimate the V_{rad} of the Earth-directed CMEs, the ESA model is able to predict the shock arrival times with accuracy comparable to most other more complex models.

1. Introduction

Earth-directed coronal mass ejections (CMEs) are able to trigger geomagnetic storms when they hit Earth's magnetosphere, provided they contain southward magnetic field component. Previous studies on the causes of geomagnetic storms have established that major geomagnetic storms are mostly caused by CMEs or their sheath regions ahead of them [see, e.g., *Gosling et al.*, 1990; *Zhang et al.*, 2007]. Therefore, a good estimate of the CME and shock arrival time at Earth is required in order to predict space weather conditions. In general, CMEs launched near the center of the solar disk arrive at Earth within 1–5 days [e.g., *Gopalswamy et al.*, 2000]. Various CME and shock propagation models have been suggested for space weather forecasting purposes. *Gopalswamy et al.* [2001] presented an empirical model that attempts to take into account that during IP propagation CME speeds converge towards the solar wind speed and that the CME acceleration ceases before 1 AU. They applied this model to a set of 47 CMEs observed during December 1996 and July 2000 and found the average prediction error of the CME arrival time to be 10.7 hours. A similar CME propagation model that considers explicitly the effect of the drag force by the solar wind on the CME has been suggested [*Vršnak*, 2001; *Vršnak and Gopalswamy*, 2002; *Borgazzi et al.*, 2009; *Vršnak et al.*, 2010]. Studies using various methods to track the CME propagation have found evidence in support of the drag force model [e.g., *Vršnak et al.*, 2004; *Byrne et al.*, 2010; *Hess and Zhang*, 2014; *Möstl et al.*, 2014]. However, validation tests of the drag model have shown that the prediction error of the disturbance arrival time at Earth is around 10 hours [e.g., *Owens and Cargill*, 2004; *Colaninno et al.*, 2013; *Vršnak et al.*, 2014], which is comparable to the result by *Gopalswamy et al.* [2001]. More recently, *Hess and Zhang* [2015] have been able to predict the arrival times of both the ejecta and the preceding sheath with the MAE of 1.5 hours and 3.5 hours, respectively, using a drag-based model. By comparison, *Möstl et al.* [2014] were able to achieve the MAE of 6.1 hours after applying an empirical correction to their predictions derived by fitting the time elongation profiles of CMEs with different geometrical models. Both these studies extend the CME measurements as far out from the Sun as possible using data from the Heliospheric Imager (HI) on the Solar TErrestrial RElations Observatory (STEREO) spacecraft. *Shi et al.* [2015] did not use HI distance measurements in their study of 21 Earth-directed CMEs, where they obtained for three different versions of the drag force model the MAE of ≈ 13 hours, which was reduced to ≈ 7–8 hours after excluding five CMEs with observed angular deflections.

A more complex model is the ENLIL model [*Odstrcil and Pizzo*, 1999; *Odstrcil et al.*, 2004], which is a 3D time-dependent MHD solar wind model that can be used to propagate CME-like structures through heliosphere. The ENLIL model is available online at the Community Coordinated Modeling Center (CCMC) at NASA Goddard Space Flight Center. The background solar wind solution needed for the ENLIL model run is provided by the Magnetohydrodynamics Around a Sphere [MAS; *Riley et al.*, 2006] or the Wang-Sheely-Arge [WSA; *Arge and Pizzo*, 2000] model. One should note that in addition to predicting the shock arrival times, the ENLIL model can be used to predict if the shock front arrives at Earth or not. *Falkenberg et al.* [2011] and *Mays et al.* [2015] used the ENLIL model to predict shock arrival times and report MAEs of 13–15 hours and 12.3 hours, respectively. However, *Taktakishvili et al.* [2009] and *Millward et al.* [2013] have obtained considerably better predictions with the ENLIL model. They reported MAEs of 5.9 hours and 7.5 hours, respectively. *Millward et al.* [2013] attribute the improvement in prediction accuracy to the CME Analysis Tool (CAT) that utilizes the three different viewpoints provided by the Solar and Heliospheric Observatory (SOHO) and STEREO spacecraft to determine the CME parameters for model input. In a separate study of CMEs causing strong geomagnetic storms *Taktakishvili et al.* [2011] determined the CME parameters using the analytical cone model [*Xie et al.*, 2004] and an automatic method [*Pulkkinen et al.*, 2010] and found MAEs of 6.9 and 11.2 hours, respectively.

Another set of models that do not use CME measurements as input parameters includes Shock Propagation Model [SPM; *Feng and Zhao*, 2006], Shock Time Arrival [STOA; *Dryer and Smart*, 1984; *Smart and Shea*, 1985] model, the Interplanetary Shock Propagation Model [ISPM; *Smith and Dryer*, 1990], and the Hakamada-Akasofu-Fry Version 2 [HAFv.2; *Fry et al.*, 2001] model. These analytical and numerical models use the location and duration of the associated soft X-ray flare and the frequency drift rate of the metric type II radio burst to derive the characteristics of the CME-driven shock near the Sun required for the model runs. A major distinction between the models is that they describe the background solar wind through which the shock propagates at different levels of detail. *Zhao and Feng* [2015] have developed a version of the SMP model that includes also the CME speed and provided the most recent comparison between the different versions of the four shock propagation models. They found that the MAEs of the shock arrival time were in the range of 8.9–10.0 h.

The CME speed can be measured most accurately from the coronagraphic observations, if the observing spacecraft has a side view of the CME. However, the Large Angle and Spectrometric Coronagraph [LASCO; *Brueckner et al.*, 1995] on the SOHO spacecraft can provide only a head-on view of the oncoming CME because SOHO spacecraft is located near Earth. Based on measurements of limb CMEs, *Schwenn et al.* [2001] reported that in general there exists a good correlation between the radial speed and the lateral expansion speed of the CME. They also suggested that the CME expansion speed could be useful for estimating the radial speed of halo CMEs, for which it is difficult to measure the latter because of unfavorable geometry. *dal Lago et al.* [2003] studied 57 limb CMEs observed by SOHO/LASCO and found an empirical relationship between the expansion and radial speed of CMEs: $V_{rad} \approx 0.88 V_{exp}$. *Schwenn et al.* [2005] studied the V_{rad}–V_{exp} relationship and suggested three plausible cone models of CME geometry, for which the V_{rad}–V_{exp} relationship depends on the cone angle. *Gopalswamy et al.* [2009a] also derived V_{rad}–V_{exp} relationships for three CME cone models and suggested that the full ice-cream cone provided the best fit with CME observations. *Michalek et al.* [2009] studied the radial and expansion speed of 256 limb CMEs observed by LASCO and found that the full cone model agrees with the observations. For the halo CME on February 15, 2011 *Gopalswamy et al.* [2012] found that the radial speed measured by the STEREO spacecraft and the speed calculated using the LASCO expansion speed and the full ice-cream cone model matched well.

The STEREO and SOHO spacecraft were viewing Earth-directed CMEs in near-quadrature during January 2010- September 2012, i.e. the coronagraphs of Sun Earth Connection Coronal and Heliospheric Investigation [SECCHI *Howard et al.*, 2008] suite on STEREO Ahead and Behind were observing Earth-directed CMEs from a side-view with minimal projection effects. This quadrature configuration of the observing spacecraft provides a unique opportunity to test the accuracy of the radial speed-expansion speed relation for Earth-directed CMEs observed by the SOHO/LASCO coronagraph. The radial speed–expansion speed relationship is useful for estimating the speed of Earth-directed CMEs when they are observed from Earth-view only. In addition, we will also test the empirical shock arrival (ESA) model proposed by *Gopalswamy et al.* [2005a] using CME propagation speeds estimated from the CME expansion speeds.

2. Data Analysis

We selected 13 CMEs with sufficient LASCO/C3 and SECCHI/COR2 observations from the list of Earth-directed CMEs in 2010-2012 published by [*Gopalswamy et al.*, 2013]. The event list of *Gopalswamy et al.* [2013] includes CMEs that (i) were seen as halo CMEs by SOHO (Earth view), (ii) had the speed $\geq$ 450 km s^{-1}, and (iii) were driving a shock at L1 as detected by the Charge, Element, and Isotope Analysis System/Mass Time-of-Flight (MTOF) experiment [*Ipavich et al.*, 1998] on SOHO. The original selection was based on LASCO halo CME alerts [see http://umbra.nascom.nasa.gov/lasco/observations/halo/; *Gopalswamy et al.*, 2010]. Some of those full halo CMEs have been later classified as partial halo CMEs in the online SOHO/LASCO CME catalog [http://cdaw.gsfc.nasa.gov/CME_list/; *Gopalswamy et al.*, 2009b]. We relaxed the *Gopalswamy et al.* [2013] criterion that accepted only halo CMEs and included also events that were reported as partial halos in the LASCO Halo Alerts. This gave us additional 6 events, increasing the total number of events on our data list to 19 events. The CME associated shocks were compiled from an online list at the SOHO MTOF web site (http://umtof.umd.edu/pm/figs.html). Table 1 lists the 19 CMEs that we selected for our study. The data in the columns 2–3 and 5 of Table 1 are compiled from the list of *Gopalswamy et al.* [2013]. The first column lists the event number and the columns 2 and 3 present the shock arrival times at SOHO and the time of the associated CME. The columns 4 and 5 give the central position angle (CPA) and the width (W) of the CME as listed in the SOHO/LASCO CME catalog. The column 6 lists the solar source of the CME (loc) in the heliographic coordinates of the eruption location as seen in EUV images either from Atmospheric Imaging Assembly [AIA; *Lemen et al.*, 2012] instrument on the Solar Dynamics Observatory (SDO) or the Extreme Ultraviolet Imager [EUVI; *Wuelser et al.*, 2004; *Howard et al.*, 2008] on STEREO. The column 7 gives the LASCO CME speed (V) in km s^{-1}. The columns 8–12 give the width (W_1 and W_2) of the CME in degrees based on two methods of estimation, the LASCO expansion speed (V_{exp}) in km s^{-1}, the radial speed V_{rad} in km s^{-1} calculated from the full ice-cream cone model using the width (W_3, column 13) of the CME in degrees as measured by the STEREO spacecraft (s/c) listed in the last column. The STEREO spacecraft for which the CME source region (flare) appeared to be closer to the limb was used for measurements. The maximum angular distance of the source region from the limb as seen from the STEREO spacecraft was 26°. Therefore the projection effects in the STEREO measurements are minimal. Calculation of the V_{rad} from the full ice-cream cone model of CMEs is discussed in Section 2.1.

For each CME we measured the lateral extent L of the CME in the LASCO/C3 field of view at the time t as shown in Figure 1 and calculated the expansion speed V_{exp} as

$$V_{exp} = \frac{\sum_{i=2}^{n} \frac{L_i - L_{i-1}}{t_i - t_{i-1}}}{n-1}, \tag{1}$$

where n is the number of measurements. The angle subtended by the measured lateral extent L was also used to estimate the width ($W2$) of the CME by setting the apex of the angle at the disk center. We do not take into account the location of the CME source on the disk. We measured the lateral extension by eye and we included only the CME main body. In the C3 image shown in Figure 1 the CME is the bright round feature extended by the blue arrow. In the coronagraphic images one can frequently see other features such as streamer deflections and sheath regions. However, shock fronts itself are impossible to see in those images because they are far too thin structures. One can only assume that the outer edge of the sheath region is the shock location. Streamer deflections are bright features visible mostly around the flanks of the CME, and they need to be excluded, when estimating the CME extent. In order to do that we have viewed movies of both direct and running difference images, while we were measuring the lateral extent of the CME, because the flank of the CME is easier to discern from movies than from single frames. Sheath regions are easier to identify in the images, because they are fainter structures surrounding the CME. In the C3 image of Figure 1, such a faint structure is visible at the opposite side of the occulting disk to the CME.

Another estimate for the width ($W1$) of the CME was calculated from a simple formula proposed by *Gopalswamy et al.* [2010] based on the correlation between the LASCO CME speed (V) and the LASCO CME width:

$$W1 = \begin{cases} 64^\circ & \text{if V} \leq 500\,\mathrm{km\,s^{-1}}, \\ 90^\circ & \text{if } 500\,\mathrm{km\,s^{-1}} < \text{V} \leq 900\,\mathrm{km\,s^{-1}}, \\ 132^\circ & \text{if V} > 900\,\mathrm{km\,s^{-1}}. \end{cases} \tag{2}$$

Figure 1 shows as an example the 4 August 2011 halo CME (event #9) that was launched from a source region at N19W36. Using LASCO images and Equation 1 we calculated the expansion speed of the CME to be 1682 km s^{-1}. The expansion speed is higher than the sky-plane speed of 1315 km s^{-1} listed in the LASCO CME Catalog. Using the LASCO sky-plane speed and Equation 2 we can estimate the CME width to be 132°. The width given by this simple formula is doubled compared to the width of 81° estimated from the STEREO-Ahead images that provide a side view of the CME.

Using the angle $W3$ as our best estimate of the CME width, because its is measured from the side view of the CME, we can evaluate the L1-based estimates $W2$ and $W2$. The linear Pearson (Spearman's rank) correlation coefficients of the angles W1 and W2 with the angle $W3$ are, 0.50 (0.50) and -0.0 (-0.06), respectively. The angles $W1$ estimated from the LASCO CME speed correlate better with the STEREO angles $W3$ than the angle $W2$ estimated from the CME extent, which provide a poor estimate of the true CME angle as expected.

2.1. V_{rad}–V_{exp} Relationship

Figure 2 shows three simple geometrical models of a CME structure and the corresponding V_{rad}–V_{exp} relationships as derived by *Gopalswamy et al.* [2009a]. Each model defines the CME as a right cone with a flat (flat cone model) or outward curved (shallow and full ice-cream cone models) bottom that corresponds to the leading edge of the CME. The length of the slant, the height, and the radius of the cone are R, r, and $l/2$, respectively. The angle w is half of the cone opening angle W, i.e. $W = 2w$. Assuming a self-similar expansion of the CME, *Gopalswamy et al.* [2009a] showed that for each model the radial speed V_{rad} equals to the expansion speed V_{exp} multiplied by a function $f(w)$ that depends only on the angle w, i.e. $V_{rad} = f(w) \times V_{exp}$.

We studied the validity of the three CME cone models by comparing the speed ratio V_{sky}/V_{exp} to the model predicted speed ratio $f(w)$ using the three different CME width estimates. The expansion speed V_{exp} was measured from the LASCO images (see Figure 1) and the radial speed V_{sky} was measured from the STEREO/COR2 images. The values are

Table 1. List of 19 Earth-directed CMEs driving a shock.

Event	Shock Time[a]	CME Time[a]	CPA[b]	W[b]	Loc[a]	V[b]	W_1	W_2	V_{exp}	V_{rad}	V_{sky}	W_3	s/c
1	2010/04/05 08:00	04/03 10:39	Halo	360	S25E00	668	90	166	868	1386	698	49	B
2	2011/02/18 00:40	02/15 02:36	Halo	360	S12W18	669	90	180	1080	1195	879	79	A
3	2011/03/10 05:45	03/07 14:48	354	261	N11E21	698	90	58	463	649	633	58	B
4	2011/06/04 19:44	06/02 07:24	Halo	360	S19E25	976	132	107	786	1217	906	51	B
5	2011/06/23 02:18	06/21 03:16	Halo	360	N16W08	719	90	133	902	1281	939	57	A
6	2011/07/11 08:08	07/09 00:48	98	225	S25E32	630	90	149	888	1418	741	49	B
7	2011/08/04 21:10	08/02 06:36	288	268	N14W15	712	90	105	826	951	570	75	A
8	2011/08/05 17:23	08/03 13:17	Halo	360	N22W30	610	90	106	1442	1328	1062	95	A
9	2011/08/05 18:32	08/04 03:40	Halo	360	N19W36	1315	132	117	1682	1826	1307	81	A
10	2011/09/09 11:49	09/06 23:05	Halo	360	N14W18	575	90	123	956	932	853	93	A
11	2011/09/17 03:05	09/14 00:00	334	242	N22W03	408	64	90	500	701	534	58	B
12	2011/11/12 05:10	11/09 13:36	Halo	360	N22E44	907	132	105	859	1091	911	66	B
13	2012/01/22 05:18	01/19 14:25	Halo	360	N32E22	1120	132	69	1038	1208	907	74	B
14	2012/01/24 14:33	01/23 03:38	Halo	360	N29W20	2157	132	93	2214	1623	1645	130	A
15	2012/03/07 03:47	03/05 04:00	Halo	360	N17E52	1531	132	76	1408	1305	636	99	B
16	2012/03/08 10:53	03/07 01:24	Halo	360	N17E27	1825	132	180	2058	1989	1866	94	B
17	2012/03/12 08:45	03/10 17:40	Halo	360	N17W24	1296	132	134	1783	1723	1361	94	A
18	2012/06/16 08:52	06/14 14:36	Halo	360	S17E06	987	132	128	1414	1290	1148	101	B
19	2012/09/30 22:21	09/28 00:12	Halo	360	N06W34	947	132	132	1385	972	967	136	A

[a] Data from *Gopalswamy et al.* [2013] except for the new events #1, #4,#6, #10, #15, and #19.

[b] Data from the LASCO CME catalog (http://cdaw.gsfc.nasa.gov/CME_list/).

listed in columns 10 and 12 of Table 1, respectively. Figure 3a shows that the speed ratios as a function of the CME width $W1$ (red triangles), $W2$ (blue squares), and $W3$ (black filled circles) fit best to predictions by the full ice-cream cone model (dashed line). The predicted speed ratios of the flat cone model (solid line) and the shallow ice-cream cone model (dotted line) both lie well below the plotted speed ratios. We also calculated the V_{rad} using the theoretical model and the width (W_3 in Table 1) of the CME measured using the STEREO/COR2 images ($W = 2w$). Figure 3b shows the scatter plot between the radial speed V_{rad} calculated using the full ice-cream cone model and the V_{sky}. The correlation coefficient was found to be 0.78. The regression line (solid line) with a slope (0.826) close to unity matches well the dashed line, which indicates a perfect match between the V_{rad} and V_{sky}. The correlation coefficient for the flat cone model and the shallow ice-cream cone model were 0.26 and 0.76, respectively. However, the slopes of the regression line were 0.685 and 0.593, respectively. For the CME width estimates $W1$ and $W2$, the correlation coefficients were 0.76 and 0.70 (full ice-cream cone model), 0.81 and 0.80 (shallow ice-cream cone model), and 0.15 and 0.31 (flat cone model), respectively . The corresponding slopes were 0.740 and 1.019 (full ice-cream cone model), 0.564 and 0.720 (shallow ice-cream cone model), and 0.665 and 0.787 (flat cone model). The correlation coefficients of the near-Sun CME speeds for the shallow ice-cream model were slightly better than those for the full ice-cream cone model, but the slopes of the regression lines differed more from unity, except for the full ice-cream cone model and the CME width $W2$. However, the correlation coefficient was lower (0.70) in that case. Therefore, we conclude that the full ice-cream cone model provides the best estimates of the V_{sky}. The overall best fit is obtained when using the CME width $W3$ from the STEREO measurement (Fig. 3b).

3. Empirical Shock Arrival Model

Predicting the arrival of the CME and the associated shock remains one of the main problems of space weather forecasting, because the SOHO/LASCO coronagraphs have only a head-on view of the Earth-directed CMEs. STEREO/SECCHI observations can provide a side-view of the Earth-directed CMEs, such as we have utilized in our study, but those observations are available only for a very limited period during the mission due to the constant drift of STEREO spacecraft around the Sun. Therefore, we have tested the prediction accuracy of the ESA model proposed by *Gopalswamy et al.* [2005a]. The ESA model is defined as

$$t = AB^{V} + C, \tag{3}$$

where t is the shock travel time in hours, V is the initial CME speed in km s^{-1}, and $A =$ 151.002, $B = 0.998625$, and $C = 11.5981$ [*Gopalswamy et al.*, 2005b]. The derivation of the ESA model takes into account the average standoff-distance of a CME-driven shock, which is the distance between the shock and its driver, i.e. the CME. The distance depends on the geometry of the driving CME and the upstream Alfvenic Mach number [see details in *Gopalswamy et al.*, 2005a]. The event-to-event variation of the CME properties and the ambient medium result in variation in the standoff distance of the shock, which can affect the arrival time of the shock front. The ESA model does not attempt to account for those effects. However, the model parameters were obtained by using CME/shock observations, therefore they do to some extent reflect the average combined effect of all significant factors affecting the shock propagation.

3.1. Shock Arrival Time Predictions

We used the ESA model together with the full ice-cream cone model (Figure 2a) of the CME to predict the shock arrival times. In order to calculate the radial speed V_{rad} from the measured expansion speed V_{exp}, we need to estimate of the half width (w) of the CME. As in Section 2, we use three different methods to estimate the CME width ($W = 2w$): (i) direct measurement from the STEREO/COR2 image (W_3 in Table 1); (ii) the width–speed relationship by *Gopalswamy et al.* [2010] (W_1 in Table 1); (iii) direct measurement of the lateral extension of the CME from the LASCO/C3 images (W_2 in Table 1; see also Figure 1). The estimation of the CME extension was made by eye. In order to get the Earth-directed radial speed the calculated speed was multiplied by $cos(\theta)cos(\phi)$, where θ is the source longitude and ϕ is the source latitude in heliographic coordinates. Table 2 lists the obtained CME speeds. The speeds $V1$, $V2$, and $V3$ in columns 4–6 are calculated using the widths W_1, W_2, and W_3 listed in Table 1. The corresponding shock travel times t_1, t_2, and t_3 are listed in columns 8–10. The differences Δt_1, Δt_2, and Δt_3 between the calculated travel times and the observed travel time t_{obs} in column 7 are given in the columns 11–13. The observed travel time of the shock t_{obs} is defined to be from the first observation time of the CME to the shock arrival time at SOHO.

Figure 4 shows the histograms for the differences Δt_1, Δt_2, and Δt_3 between the calculated travel times and the observed travel time t_{obs}. The mean absolute error (MAE) is 8.4 hours, if we use the ESA model and the CME speed estimate based on the STEREO/COR2 measurements of the CME width (W_3 in Table 1). If the CME width estimation is based on the LASCO measurements only (W_1 in Table 1 from Equation 2 or W_2 in Table 1 from the LASCO/C3 lateral extension measurement) the MAE values are 14.0 hours and 16.4 hours, respectively. The respective root mean square errors (RM-

Table 2. Shock travel times

Event	Shock Time[a]	CME Time[a]	V_1	V_2	V_3	t_{obs}[b]	t_1	t_2	t_3	Δt_1	Δt_2	Δt_3
1	2010/04/05 08:00	04/03 10:39	793	445	1266	45.4	62.3	93.4	38.0	17.0	48.1	-7.3
2	2011/02/18 00:40	02/15 02:36	1005	502	1112	70.1	49.5	87.2	44.3	-20.6	17.2	-25.8
3	2011/03/10 05:45	03/07 14:48	424	595	595	63.0	95.8	78.2	78.2	32.9	15.3	15.3
4	2011/06/04 19:44	06/02 07:24	487	586	1043	59.5	88.9	79.0	47.6	28.6	18.7	-12.8
5	2011/06/23 02:18	06/21 03:16	859	616	1220	47.0	57.9	76.3	39.8	10.9	29.3	-7.3
6	2011/07/11 08:08	07/09 00:48	683	436	1090	55.3	70.6	45.3	55.9	15.3	39.1	-10.0
7	2011/08/04 21:10	08/02 06:36	774	684	891	62.6	63.6	70.5	55.9	1.1	7.9	-6.7
8	2011/08/05 17:23	08/03 13:17	1158	1015	1110	52.1	42.3	49.0	44.4	-9.8	-3.1	-7.7
9	2011/08/05 18:32	08/04 03:40	930	1038	1397	38.9	53.6	47.8	33.7	14.7	9.0	-5.2
10	2011/09/09 11:49	09/06 23:05	882	681	860	60.7	56.5	70.8	57.8	-4.3	10.1	-2.9
11	2011/09/17 03:05	09/14 00:00	602	463	649	75.1	77.6	91.5	73.4	2.5	16.4	-1.7
12	2011/11/12 05:10	11/09 13:36	414	506	728	63.6	97.0	86.8	67.1	33.5	23.3	3.5
13	2012/01/22 05:18	01/19 14:25	590	1002	950	62.9	78.7	49.6	52.5	15.8	-13.2	-10.4
14	2012/01/24 14:33	01/23 03:38	1315	1773	1334	34.9	36.3	24.8	35.7	1.4	-10.2	0.8
15	2012/03/07 03:47	03/05 04:00	599	945	768	47.6	77.8	52.7	64.1	30.0	5.0	16.3
16	2012/03/08 10:53	03/07 01:24	1267	877	1695	33.5	38.0	56.8	26.3	4.5	23.3	-7.2
17	2012/03/12 08:45	03/10 17:40	1126	1109	1505	39.1	43.7	44.4	30.6	4.6	5.3	-8.5
18	2012/06/16 08:52	06/14 14:36	972	1000	1227	42.3	51.3	49.7	39.5	9.0	7.5	-2.8
19	2012/09/30 22:21	09/28 00:12	825	825	801	70.2	60.1	60.1	61.7	-10.0	-10.0	-8.4

[a] Same data as in Table 1.

[b] Data from *Gopalswamy et al.* [2013] except for the new events #1, #4,#6, #10, #15, and #19.

SEs) are 5.8 hours ($W3$), 10.4 hours ($W2$), and 11.6 hours ($W1$). The best prediction for the shock travel time is obtained by the ESA model when the CME width is measured using the STEREO/COR2 observations. The MAE of 8.4 hours for our set of 19 events is larger than the MAE of 7.3 hours reported by *Gopalswamy et al.* [2013] for their set of 20 CMEs. Our prediction error would be smaller (MAE=7.5 hours), if we exclude the 2011 February 18 shock event (event #2) for which the arrival time was estimated to be 25.8 hours too early. The details of the associated CME together with another outlier CME on 2012 July 12, which is not in our event list, are discussed in *Gopalswamy et al.* [2013], who excluded both of these events. They note that the associated CME on 2011 February 15 was preceded by 11 CMEs within a 32-hour period. They suggests that the slower preceding CMEs increased the effective drag on the 2011 February 15 CME, hence it arrived significantly later than predicted by the ESA model. Table 3 lists the errors for all models and CME width estimates used in our analysis. From Table 3 it is clear that the MAEs for the ESA model predictions calculated from the shallow ice-cream cone model or flat cone model using the CME width estimates derived from SOHO ($W1$ and $W2$) or the STEREO ($W3$) observations are significantly larger.

4. Discussion and Conclusions

First we tested the validity of the V_{rad}–V_{exp} relationships derived using the simple geometrical cone models of the CME derived by *Gopalswamy et al.* [2009a] (see Figure 2). Our data set consisted of 19 Earth-directed CMEs observed by both SOHO and STEREO spacecraft during January 2010-September 2012, when the spacecraft were in near-quadrature [*Gopalswamy et al.*, 2013]. During the study period, the STEREO/COR2 observations provided a side-view of the selected CMEs with minimal projection effects.

Our comparison of the ratio of the CME radial speeds measured from the STEREO/COR2 observations and the CME expansion speeds measured from the LASCO/C3 observations to the model predictions showed that the best match is obtained for the full ice-cream model. Our result is in accordance with the results obtained by *Michalek et al.* [2009], who studied 256 limb CMEs for which they estimated the CME widths from the LASCO/C3 lateral extension measurements. They divided the CMEs into seven 20° bins and showed that the ratio of the average measured radial speed and the average calculated expansion speed in each group follows the prediction by the full ice-cream cone model. Similar conclusion was reached by *Gopalswamy et al.* [2012] who studied the halo CME on 15 February 2011. Therefore, we conclude that the full ice-cream cone model of the CME should be used for estimating the CME radial speed from the CME expansion speed.

Secondly we tested the accuracy of shock propagation model (the ESA model) proposed by *Gopalswamy et al.* [2005a], when the CME radial speed is estimated using the full ice-cream model of the CME. We used three different methods to measure the CME width, which is the required input for the CME model. We measured the CME width (i) directly from the STEREO/COR2 images (ii) from the simple CME width–speed relationship (Equation 2) suggested by *Gopalswamy et al.* [2010] and (iii) from the direct measurement of the CME lateral extent in the LASCO/C3 images. Our results showed that the best prediction accuracy is achieved when the STEREO/COR2 width measurement are used. In that case the MAE between the observed travel time of the shock and the ESA predicted travel time is 8.4 hours and the RMSE is 5.8 hours. If we use the LASCO measurements to estimate the CME width (either from Equation 2 or from direct CME lateral extent measurement), then the MAEs increase by 1.7 and 2.0 times (14.0 hours and 16.4 hours), respectively. The RMSEs also increase to 10.4 hours and 11.6 hours, respectively.

In a recent study, *Shanmugaraju et al.* [2015] suggested a shock travel time model where the shock transit time dependence on the CME speed only. The comparison with the ESA model (see their Figure 3) shows that both models predict similar shock transit times for CMEs with a speed ≥ 600 km s^{-1}. For slower-speed CMEs, the model by *Shanmugaraju et al.* [2015] predicts shorter travel times than the ESA model. *Falkenberg et al.* [2011] analyzed 16 shock fronts identified at Mars from Mars Global Surveyor observations and at Earth from OMNI data in 2001 and 2003, when the separation between Earth and Mars was $< 80°$ in heliocentric longitude. They identified the associated CME driving the shock from the SOHO/LASCO catalogue and modelled the CME propagation by running the ENLILv2.6 model for which the MAS or WSA models provided the coronal solar wind solution. The four of the six CME input parameters to the model (time, speed, direction and angular width) were obtained using either the manual method by *Xie et al.* [2004] or the automated method by *Pulkkinen et al.* [2010]. The other two parameters, the CME density and temperature, were set to the standard values of 1200 cm^3 and 0.8 MK, respectively. *Falkenberg et al.* [2011] found that the MAEs of the shock arrival times at Earth simulated with ENLILv2.6 were 13 hours (manual method) and 15 hours (automated method). In another study of 36 strong geomagnetic storm events, *Taktakishvili et al.* [2011] were able to drive the input parameters for 20 CMEs out of the 36 CMEs using the same methods of *Xie et al.* [2004] and *Pulkkinen et al.* [2010]. They used the two sets of CME inputs to simulate the shock propagation with the WSA-ENLIL model and obtained the MAEs of 6.9 and 11.2 hours, respectively. In addition, they analyzed the events using the ESA model for which the MAE was 8.0 hours. These results are comparable to previous study by *Taktakishvili et al.* [2009] were they used the WSA-ENLIL model with the CME parameters obtained from the cone model of *Xie et al.* [2004] and the ESA model to predict the shock arrival times for a set of 14 mainly fast CMEs that occurred between August 2000 and December 2006. In this study they found the MAE for the ENLIL model to be 5.9 hours and that for the ESA model 8.4 hours. *Millward et al.* [2013] obtained a slightly lower prediction accuracy (7.5 hours) for the WSA-ENLIL model in a study of 25 CMEs observed during October 2011–October 2012. They analyzed multi-viewpoint CME observations provided by the SOHO and STEREO spacecraft using the CAT software, which is in routine use at the NOAA Space Weather Prediction Center (SWPC), to improve their CME input parameter estimation. Recently *Mays et al.* [2015] made ensemble predictions of the CME-driven shock or the disturbance arrival times using WSA-ENLIL+Cone model for a set of 30 CMEs observed during January 2013–July 2014. They found the MAE and the RMSE of the ensemble predictions to be 12.3 hours and 13.9 hours, respectively. These errors are comparable to the errors reported by *Falkenberg et al.* [2011]. The ENLIL model seems to be able to provide slightly better prediction accuracy than the ESA model, if the CME input parameters can be estimated sufficiently precisely.

Hess and Zhang [2015] modeled the shock propagation with a drag-based model that also extends the CME measurements as far out from the Sun as possible using STEREO/HI data. They predicted the arrival times of both the ejecta and the preceding sheath with the MAE of 1.5 and 3.5 hours, respectively. However, the studied set of events included only seven CMEs. In another study using the STEREO/HI data, *Möstl et al.* [2014] fitted the time–elongation measurements of CMEs using geometrical models that assume different shapes for the shock front and they also assumed a constant CME speed and propagation direction. They studied 22 CMEs and were able to reduce the MAE from 8.1 hours down to 6.1 hours by applying an empirical correction to their initial predictions. Extending the CME measurements farther out from the Sun naturally improves the accuracy of the shock arrival predictions, but it also reduces the lead time of the prediction. *Möstl et al.* [2014] report an average lead time of 26.4 hours for the 22 CMEs (range from -53.6 to +0.28 hours) and *Hess and Zhang* [2015] mention that in their study the lead time counted from the time of the last SECCHI image used for the CME measurement was at least 36 hours. Assuming that the CME images can be transmitted promptly for ground analysis, the lead times are mostly feasible. Clearly the model by *Hess and Zhang* [2015] performs better than our simple ESA model. The geometrical models analyzed by *Möstl et al.* [2014] provide comparable or slightly better accuracy.

A widely used group of shock arrival time prediction models do not use input parameters derived from CME measurements. Instead input parameters for the near-Sun shock are derived from the drift rate of type II solar radio burst, the duration of soft X-ray flare, and the source location of the flare. In addition, the speed and density of the background solar wind is modeled with varying levels of detail. Similar to the ENLIL model, these models can predict if the shock arrives at Earth or not. *Zhao and Feng* [2015] reported on the results of their updated version of the Shock Propagation Model (SPM3). They found that the MAE of the shock travel times predicted by the SPM3 is 9.1 hours. They also compared the SMP3 results with the predictions of other models such as the STOA [*Dryer and Smart*, 1984; *Smart and Shea*, 1985] model, the ISPM [*Smith and Dryer*, 1990], and the HAFv.2 [*Fry et al.*, 2001] model and also with the earlier version of their own model called SMP2 (see their Table 4). They found that the MAEs of all models ranged from 8.87 hours to 10.04 hours. *Liu and Qin* [2015] used the STOA model to study 220 solar eruption events with a shock at Earth during the solar cycle 23. The RMSE of the STOA model was 18.26 hours and 17.88 hours for a modified STOA model. Compared to the results of these physics-based solar-eruption-driven models, our predictions of the shock arrival times are comparable.

We conclude that the full ice-cream cone model of the CME is the best model to estimate the CME radial speed from the CME expansion speed. We also note that all the other MAEs reported for the ESA model in earlier studies are comparable to our results of 8.4 hours that was obtained using the CME width derived from the STEREO measurements in near-quadrature. The prediction error of the ESA model increases up to 14.0–16.4 hours, if the CME width is derived from SOHO observations only. When the results of the ESA model are compared with those obtained with the ENLIL model, the errors in the arrival time predictions by the considerably simpler ESA model seem are slightly larger (0.9–2.5 hours) than the most accurate results reported for the ENLIL model. However, it appears that if the CME parameters are not selected carefully, the prediction accuracy of the ENLIL model decreases into 11–15 hours. The best prediction accuracy of 3.5 hours was obtained for the sheath arrival time with a drag-based model by *Hess and Zhang* [2015]. The other geometrical and physics based models provide results that are comparable to the results of the ESA model based on the STEREO observations in near-quadrature. Based on comparisons of the ESA model predictions of the shock arrival times with those of other models, we can conclude that the ESA model using the

STEREO measurements is able to predict the shock arrivals with a comparable or in some cases even with a better accuracy, excluding the recent drag-based model and those based the ENLIL model obtained by *Taktakishvili et al.* [2009, 2011] and *Millward et al.* [2013].

Acknowledgments. We thank the SOHO/LASCO and STEREO/SECCHI teams for providing the data. SOHO is an international cooperation project between ESA and NASA. This research was supported by NASA's Living with a Star TR&T Program. P.M. was partially supported by NSF grant AGS-1358274.

References

Arge, C. N., and V. J. Pizzo (2000), Improvement in the prediction of solar wind conditions using near-real time solar magnetic field updates, *J. Geophys. Res.*, *105*, 10465–10480, doi:10.1029/1999JA000262.

Borgazzi, A., A. Lara, E. Echer, and M. V. Alves (2009), Dynamics of coronal mass ejections in the interplanetary medium, *Astron. Astrophys. 498*, 885–889, doi:10.1051/0004-6361/200811171.

Brueckner, G. E., R. A. Howard, M. J. Koomen, C. M. Korendyke, D. J. Michels, J. D. Moses, D. G. Socker, K. P. Dere, P. L. Lamy, A. Llebaria, M. V. Bout, R. Schwenn, G. M. Simnett, D. K. Bedford, and C. J. Eyles (1995), The Large Angle Spectroscopic Coronagraph (LASCO), *Sol. Phys.*, *162*, 357–402, doi:10.1007/BF00733434.

Byrne, J. P., S. A. Maloney, R. T. J. McAteer, J. M. Refojo, and P. T. Gallagher (2010), Propagation of an Earth-directed coronal mass ejection in three dimensions, *Nature Communications*, *1*, 74, doi:10.1038/ncomms1077.

Colaninno, R. C., A. Vourlidas, and C. C. Wu (2013), Quantitative comparison of methods for predicting the arrival of coronal mass ejections at Earth based on multiview imaging, *J. Geophys. Res.*, *118*, 6866–6879, doi:10.1002/2013JA019205.

dal Lago, A., R. Schwenn, and W. D. Gonzalez (2003), Relation between the radial speed and the expansion speed of coronal mass ejections, *Adv. Space Res.*, *32*, 2637–2640, doi:10.1016/j.asr.2003.03.012.

Dryer, M., and D. F. Smart (1984), Dynamical models of coronal transients and interplanetary disturbances, *Adv. Space Res.*, *4*, 291–301, doi:10.1016/0273-1177(84)90573-8.

Falkenberg, T. V., A. Taktakishvili, A. Pulkkinen, S. Vennerstrom, D. Odstrcil, D. Brain, G. Delory, and D. Mitchell (2011), Evaluating predictions of ICME arrival at Earth and Mars, *Space Weather*, *9*, S00E12, doi:10.1029/2011SW000682.

Feng, X., and X. Zhao (2006), A New Prediction Method for the Arrival Time of Interplanetary Shocks, *Sol. Phys.*, *238*, 167–186, doi:10.1007/s11207-006-0185-3.

Fry, C. D., W. Sun, C. S. Deehr, M. Dryer, Z. Smith, S.-I. Akasofu, M. Tokumaru, and M. Kojima (2001), Improvements to the HAF solar wind model for space weather predictions, *J. Geophys. Res.*, *106*, 20985–21002, doi:10.1029/2000JA000220.

Gopalswamy, N., A. Lara, R. P. Lepping, M. L. Kaiser, D. Berdichevsky, and O. C. St. Cyr (2000), Interplanetary acceleration of coronal mass ejections, *Geophys. Res. Lett. 27*, 145–148, doi:10.1029/1999GL003639.

Gopalswamy, N., A. Lara, S. Yashiro, M. L. Kaiser, and R. A. Howard (2001), Predicting the 1-AU arrival times of coronal mass ejections, *J. Geophys. Res. 106*, 29207–29218, doi:10.1029/2001JA000177.

Gopalswamy, N., A. Lara, P. K. Manoharan, and R. A. Howard (2005a), An empirical model to predict the 1-AU arrival of interplanetary shocks, *Adv. Space Res.*, *36*, 2289–

2294, doi:10.1016/j.asr.2004.07.014.

Gopalswamy, N., S. Yashiro, Y. Liu, G. Michalek, A. Vourlidas, M. L. Kaiser, and R. A. Howard (2005b), Coronal mass ejections and other extreme characteristics of the 2003 October-November solar eruptions, *J. Geophys. Res.*, *110*, A09S15, doi: 10.1029/2004JA010958.

Gopalswamy, N., A. dal Lago, S. Yashiro, and S. Akiyama (2009a), The Expansion and Radial Speeds of Coronal Mass Ejections, *Cent. Eur. Aphys. Bull.*, *33*, 115–124.

Gopalswamy, N., S. Yashiro, G. Michalek, G. Stenborg, A. Vourlidas, S. Freeland, and R. Howard (2009b), The SOHO/LASCO CME Catalog, *Earth Moon and Planets*, *104*, 295–313, doi:10.1007/s11038-008-9282-7.

Gopalswamy, N., S. Yashiro, G. Michalek, H. Xie, P. Mäkelä, A. Vourlidas, and R. A. Howard (2010), A Catalog of Halo Coronal Mass Ejections from SOHO, *Sun and Geosphere*, *5*, 7–16.

Gopalswamy, N., P. Mäkelä, S. Yashiro, and J. M. Davila (2012), The Relationship Between the Expansion Speed and Radial Speed of CMEs Confirmed Using Quadrature Observations of the 2011 February 15 CME, *Sun and Geosphere*, *7*, 7–11.

Gopalswamy, N., P. Mäkelä, H. Xie, and S. Yashiro (2013), Testing the empirical shock arrival model using quadrature observations, *Space Weather*, *11*, 661–669, doi: 10.1002/2013SW000945.

Gosling, J. T., S. J. Bame, D. J. McComas, and J. L. Phillips (1990), Coronal mass ejections and large geomagnetic storms, *Geophys. Res. Lett.*, *17*, 901–904, doi: 10.1029/GL017i007p00901.

Hess, P., and J. Zhang (2014), Stereoscopic Study of the Kinematic Evolution of a Coronal

Mass Ejection and Its Driven Shock from the Sun to the Earth and the Prediction of Their Arrival Times, *Astrophys. J.*, *792*, 49, doi:10.1088/0004-637X/792/1/49.

Hess, P., and J. Zhang (2015), Predicting CME Ejecta and Sheath Front Arrival at L1 with a Data-Constrained Physical Model, *Astrophys. J.*, *812*, 144, doi:10.1088/0004-637X/812/2/144.

Howard, R. A., J. D. Moses, A. Vourlidas, J. S. Newmark, D. G. Socker, S. P. Plunkett, C. M. Korendyke, J. W. Cook, A. Hurley, J. M. Davila, W. T. Thompson, O. C. St Cyr, E. Mentzell, K. Mehalick, J. R. Lemen, J. P. Wuelser, D. W. Duncan, T. D. Tarbell, C. J. Wolfson, A. Moore, R. A. Harrison, N. R. Waltham, J. Lang, C. J. Davis, C. J. Eyles, H. Mapson-Menard, G. M. Simnett, J. P. Halain, J. M. Defise, E. Mazy, P. Rochus, R. Mercier, M. F. Ravet, F. Delmotte, F. Auchere, J. P. Delaboudiniere, V. Bothmer, W. Deutsch, D. Wang, N. Rich, S. Cooper, V. Stephens, G. Maahs, R. Baugh, D. McMullin, and T. Carter (2008), Sun Earth Connection Coronal and Heliospheric Investigation (SECCHI), *Space Sci. Rev.*, *136*, 67–115, doi:10.1007/s11214-008-9341-4.

Ipavich, F. M., A. B. Galvin, S. E. Lasley, J. A. Paquette, S. Hefti, K.-U. Reiche, M. A. Coplan, G. Gloeckler, P. Bochsler, D. Hovestadt, H. Grünwaldt, M. Hilchenbach, F. Gliem, W. I. Axford, H. Balsiger, A. Bürgi, J. Geiss, K. C. Hsieh, R. Kallenbach, B. Klecker, M. A. Lee, G. G. Managadze, E. Marsch, E. Möbius, M. Neugebauer, M. Scholer, M. I. Verigin, B. Wilken, and P. Wurz (1998), Solar wind measurements with SOHO: The CELIAS/MTOF proton monitor, *J. Geophys. Res.*, *103*, 17205–17214, doi:10.1029/97JA02770.

Lemen, J. R., A. M. Title, D. J. Akin, P. F. Boerner, C. Chou, J. F. Drake, D. W. Duncan, C. G. Edwards, F. M. Friedlaender, G. F. Heyman, N. E. Hurlburt, N. L. Katz, G. D.

Kushner, M. Levay, R. W. Lindgren, D. P. Mathur, E. L. McFeaters, S. Mitchell, R. A. Rehse, C. J. Schrijver, L. A. Springer, R. A. Stern, T. D. Tarbell, J.-P. Wuelser, C. J. Wolfson, C. Yanari, J. A. Bookbinder, P. N. Cheimets, D. Caldwell, E. E. Deluca, R. Gates, L. Golub, S. Park, W. A. Podgorski, R. I. Bush, P. H. Scherrer, M. A. Gummin, P. Smith, G. Auker, P. Jerram, P. Pool, R. Soufli, D. L. Windt, S. Beardsley, M. Clapp, J. Lang, and N. Waltham (2012), The Atmospheric Imaging Assembly (AIA) on the Solar Dynamics Observatory (SDO), *Sol. Phys.*, *275*, 17–40, doi:10.1007/s11207-011-9776-8.

Jang, S., Y.-J. Moon, J.O., Lee, and H. Na (2014), Comparison of interplanetary CME arrival times and solar wind parameters based on the WSA-ENLIL model with three cone types and observations, *J. Geophys. Res.*, *119*, 7120–7127, doi:10.1002/2014JA020339.

Liu, H.-L., and G. Qin (2015), Improvements of the shock arrival times at the Earth model STOA, *J. Geophys. Res.*, *120*, 5290–5297, doi:10.1002/2015JA021072.

Mays, M. L., A. Taktakishvili, A. Pulkkinen, P. J. MacNeice, L. Rastätter, D. Odstrcil, L. K. Jian, I. G. Richardson, J. A. LaSota, Y. Zheng, and M. M. Kuznetsova (2015), Ensemble Modeling of CMEs Using the WSA-ENLIL+Cone Model, *Sol. Phys.*, *290*, 1775–1814, doi:10.1007/s11207-015-0692-1.

Michalek, G., N. Gopalswamy, and S. Yashiro (2009), Expansion Speed of Coronal Mass Ejections, *Sol. Phys.*, *260*, 401–406, doi:10.1007/s11207-009-9464-0.

Millward, G., D. Biesecker, V. Pizzo, and C. A. de Konig (2013), An operational software tool for the analysis of coronagraph images: Determining CME parameters for input into the WSA-Enlil heliospheric model, *Space Weather*, *11*, 57–68, doi:10.1002/swe.20024.

Möstl, C., K. Amla, J. R. Hall, P. C. Liewer, E. M. De Jong, R. C. Colaninno, A. M.

Veronig, T. Rollett, M. Temmer, V. Peinhart, J. A. Davies, N. Lugaz, Y. D. Liu, C. J. Farrugia, J. G. Luhmann, B. Vršnak, R. A. Harrison, and A. B. Galvin (2014), Connecting Speeds, Directions and Arrival Times of 22 Coronal Mass Ejections from the Sun to 1 AU, *Astrophys. J.*, *787*, 119, doi:10.1088/0004-637X/787/2/119.

Odstrcil, D., and V. J. Pizzo (1999), Distortion of the interplanetary magnetic field by three-dimensional propagation of coronal mass ejections in a structured solar wind, *J. Geophys. Res.*, *104*, 28225–28240, doi:10.1029/1999JA900319.

Odstrcil, D., P. Riley, and X. P. Zhao (2004), Numerical simulation of the 12 May 1997 interplanetary CME event, *J. Geophys. Res.*, *109*, A02116, doi:10.1029/2003JA010135.

Owens, M., and P. Cargill (2004), Predictions of the arrival time of Coronal Mass Ejections at 1AU: an analysis of the causes of errors, *Ann. Geophys.*, *22*, 661–671, doi:10.5194/angeo-22-661-2004.

Pulkkinen, A., T. Oates, and A. Taktakishvili (2010), Automatic Determination of the Conic Coronal Mass Ejection Model Parameters, *Sol. Phys.*, *261*, 115–126, doi:10.1007/s11207-009-9473-z.

Riley, P., J. A. Linker, Z. Mikić, R. Lionello, S. A. Ledvina, and J. G. Luhmann (2006), A Comparison between Global Solar Magnetohydrodynamic and Potential Field Source Surface Model Results, *Astrophys. J.*, *653*, 1510–1516, doi:10.1086/508565.

Schwenn, R., A. dal Lago, W. D. Gonzalez, E. Huttunen, C. O. St.Cyr, and S. P. Plunkett (2001), A Tool For Improved Space Weather Predictions: The CME Expansion Speed, *AGU Fall Meeting Abstracts*, p. A739.

Schwenn, R., A. dal Lago, E. Huttunen, and W. D. Gonzalez (2005), The association of coronal mass ejections with their effects near the Earth, *Ann. Geophys.*, *23*, 1033–1059, doi:10.5194/angeo-23-1033-2005.

Shanmugaraju, A., M. Syed Ibrahim, Y.-J. Moon, K. Kasro Lourdhina, and M. Dharanya (2015), Arrival time of solar eruptive CMEs associated with ICMEs of magnetic cloud and ejecta, *Astrophys. Space Sci.*, *357*, 69, doi:10.1007/s10509-015-2251-5.

Shi, T., Y. Wang, L. Wan, X. Cheng, M. Ding and J. Zhang (2015), Predicting the Arrival Time of Coronal Mass Ejections with the Graduated Cylindrical Shell and Drag Force Model, *Astrophys. J.*, *806*, 271, doi:10.1088/0004-637X/806/2/271

Smart, D. F., and M. A. Shea (1985), A simplified model for timing the arrival of solar flare-initiated shocks, *J. Geophys. Res.*, *90*, 183–190, doi:10.1029/JA090iA01p00183.

Smith, Z., and M. Dryer (1990), MHD study of temporal and spatial evolution of simulated interplanetary shocks in the ecliptic plane within 1 AU, *Sol. Phys.*, *129*, 387–405, doi: 10.1007/BF00159049.

Taktakishvili, A., M. Kuznetsova, P. MacNeice, M. Hesse, L. Rastätter, A. Pulkkinen, A. Chulaki, and D. Odstrcil (2009), Validation of the coronal mass ejection predictions at the Earth orbit estimated by ENLIL heliosphere cone model, *Space Weather*, *7*, S03004, doi:10.1029/2008SW000448.

Taktakishvili, A., A. Pulkkinen, P. MacNeice, M. Kuznetsova, M. Hesse, and D. Odstrcil (2011), Modeling of coronal mass ejections that caused particularly large geomagnetic storms using ENLIL heliosphere cone model, *Space Weather*, *9*, S06002, doi: 10.1029/2010SW000642.

Vršnak, B. (2001), Deceleration of Coronal Mass Ejections, *Sol. Phys.*, *202*, 173–189, doi:10.1023/A:1011833114104.

Vršnak, B., and N. Gopalswamy (2002), Influence of the aerodynamic drag on the motion of interplanetary ejecta, *J. Geophys. Res.*, *107*, 1019, doi:10.1029/2001JA000120.

Vršnak, B., D. Ruždjak, D. Sudar, and N. Gopalswamy (2004), Kinematics of coronal mass ejections between 2 and 30 solar radii. What can be learned about forces governing the eruption?, *Astron. Astrophys.*, *423*, 717–728, doi:10.1051/0004-6361:20047169.

Vršnak, B., T. Žic, T. V. Falkenberg, C. Möstl, S. Vennerstrom, and D. Vrbanec (2010), The role of aerodynamic drag in propagation of interplanetary coronal mass ejections, *Astron. Astrophys.*, *512*, A43, doi:10.1051/0004-6361/200913482.

Vršnak, B., M. Temmer, T. Žic, A. Taktakishvili, M. Dumbović, C. Möstl, A. M. Veronig, M. L. Mays, and D. Odstrčil (2014), Heliospheric Propagation of Coronal Mass Ejections: Comparison of Numerical WSA-ENLIL+Cone Model and Analytical Drag-based Model, *Astrophys. J. (Supp.)*, *213*, 21, doi:10.1088/0067-0049/213/2/21.

Wuelser, J.-P., J. R. Lemen, T. D. Tarbell, C. J. Wolfson, J. C. Cannon, B. A. Carpenter, D. W. Duncan, G. S. Gradwohl, S. B. Meyer, A. S. Moore, R. L. Navarro, J. D. Pearson, G. R. Rossi, L. A. Springer, R. A. Howard, J. D. Moses, J. S. Newmark, J.-P. Delaboudiniere, G. E. Artzner, F. Auchere, M. Bougnet, P. Bouyries, F. Bridou, J.-Y. Clotaire, G. Colas, F. Delmotte, A. Jerome, M. Lamare, R. Mercier, M. Mullot, M.-F. Ravet, X. Song, V. Bothmer, and W. Deutsch (2004), EUVI: the STEREO-SECCHI extreme ultraviolet imager, in *Telescopes and Instrumentation for Solar Astrophysics*, *Society of Photo-Optical Instrumentation Engineers (SPIE) Conference Series*, vol. 5171, edited by S. Fineschi and M. A. Gummin, pp. 111–122, doi:10.1117/12.506877.

Xie, H., L. Ofman, and G. Lawrence (2004), Cone model for halo CMEs: Application to space weather forecasting, *J. Geophys. Res.*, *109*, A03109, doi:10.1029/2003JA010226.

Zhang, J., I. G. Richardson, D. F. Webb, N. Gopalswamy, E. Huttunen, J. C. Kasper,

N. V. Nitta, W. Poomvises, B. J. Thompson, C.-C. Wu, S. Yashiro, and A. N. Zhukov (2007), Solar and interplanetary sources of major geomagnetic storms (Dst $\leq$ -100 nT) during 1996-2005, *J. Geophys. Res.*, *112*(A11), A10102, doi:10.1029/2007JA012321.

Zhao, X. H., and X. S. Feng (2015), Influence of a CME's Initial Parameters on the Arrival of the Associated Interplanetary Shock at Earth and the Shock Propagational Model Version 3, *Astrophys. J.*, *809*, 44, doi:10.1088/0004-637X/809/1/44.

Žic, T., B. Vršnak, and M. Temmer (2015) Heliospheric Propagation of Coronal Mass Ejections: Drag-Based Model Fitting, *Astrophys. J. Suppl. S.*, *218*, 32, doi:10.1088/0067-0049/218/2/32

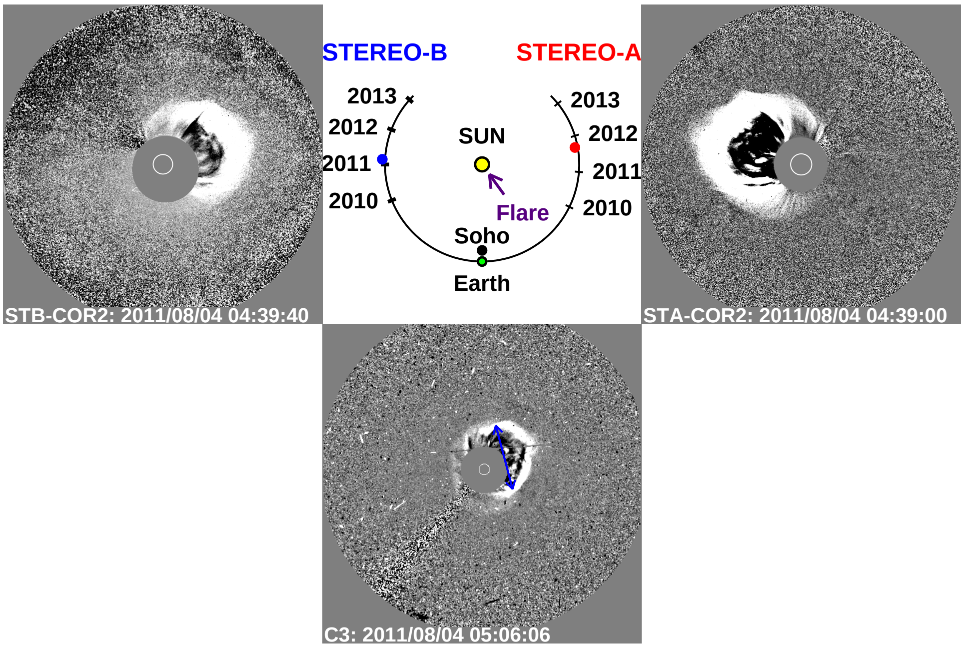

Figure 1. The 2011 August 4 CME as observed by COR2 and C3 coronagraphs on the STEREO and SOHO spacecraft. The running difference images shown are for STEREO-B/COR2 (top left), STEREO-A/COR2 (top right) and SOHO/C3 (bottom). The blue double-headed arrow marks the lateral extent of the CME in the C3 field of view. The schematic plot at the middle shows the relative locations of the spacecraft and the arrow points to the flare location at the Sun.

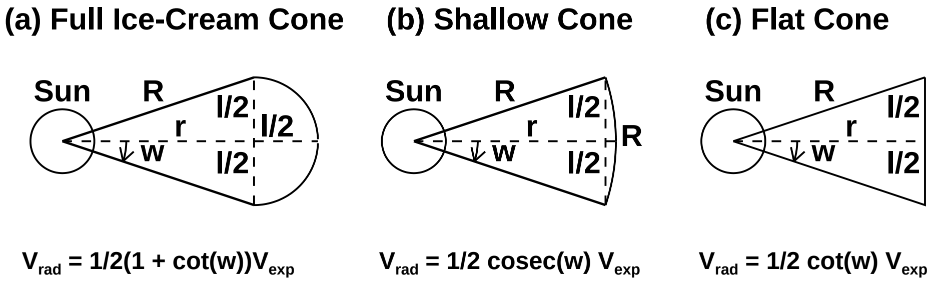

Figure 2. Different CME cone models and the corresponding V_{rad}–V_{exp} relationships (adapted from *Gopalswamy et al.* [2009a]).

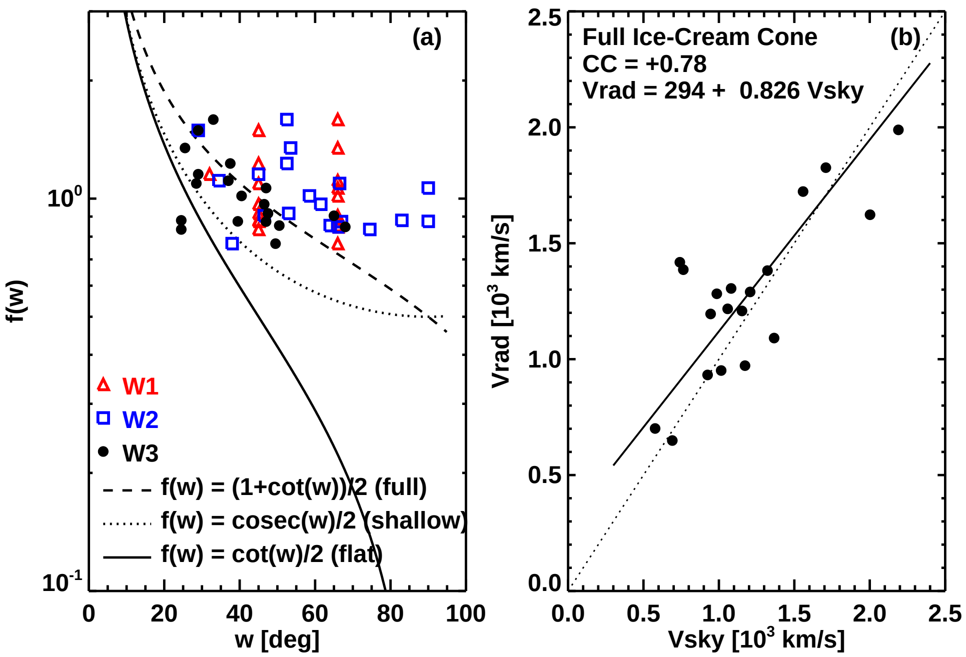

Figure 3. (a) Comparison of the speed ratio $f(w) = V_{rad}/V_{exp}$ to the predicted ratios of the three CME models of Figure 2 using the three different CME width estimates. The angle w is half of the cone opening angle ($W1$, $W2$ and $W3$ in Table 1). (b) The measured SECCHI/COR2 radial speed V_{sky} versus the radial speed V_{rad} calculated using the full ice-cream cone model shown in Figure 2a and the CME width $W3$ obtained from the STEREO observations. The correlations coefficient and the equation of the regression line (solid line) are plotted on the figure. The dashed line correspond the line $V_{rad} = V_{sky}$.

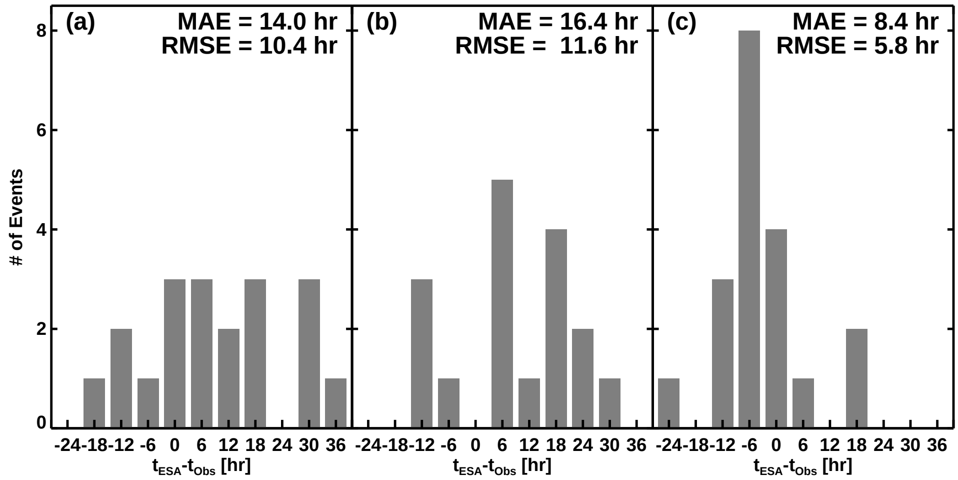

Figure 4. Differences between the observed travel time of the shock (t_{obs}) and the shock travel times (t_{ESA}) predicted by the ESA model. The CME speed was calculated from the full ice-cream cone model using the CME width (a) from the formula suggested by *Gopalswamy et al.* [2010] using the CME catalog speed (W_1 in Table 1), (b) from the direct LASCO/C3 lateral extension measurement (W_2 in Table 1) and (c) the direct STEREO/COR2 measurements (W_3 in Table 1). MAE stands for the mean absolute error and RMSE for the root mean square error.

Table 3. The RMSE and MAE values in hours.

CME	Full Ice-Cream Cone		Shallow Ice-Cream Cone		Flat Cone	
Width	MAE	RMSE	MAE	RMSE	MAE	RMSE
$W1$	14.0	10.4	25.7	13.6	54.6	18.3
$W2$	16.4	11.6	26.4	13.8	61.6	27.7
$W3$	8.4	5.8	12.7	8.3	28.7	15.3

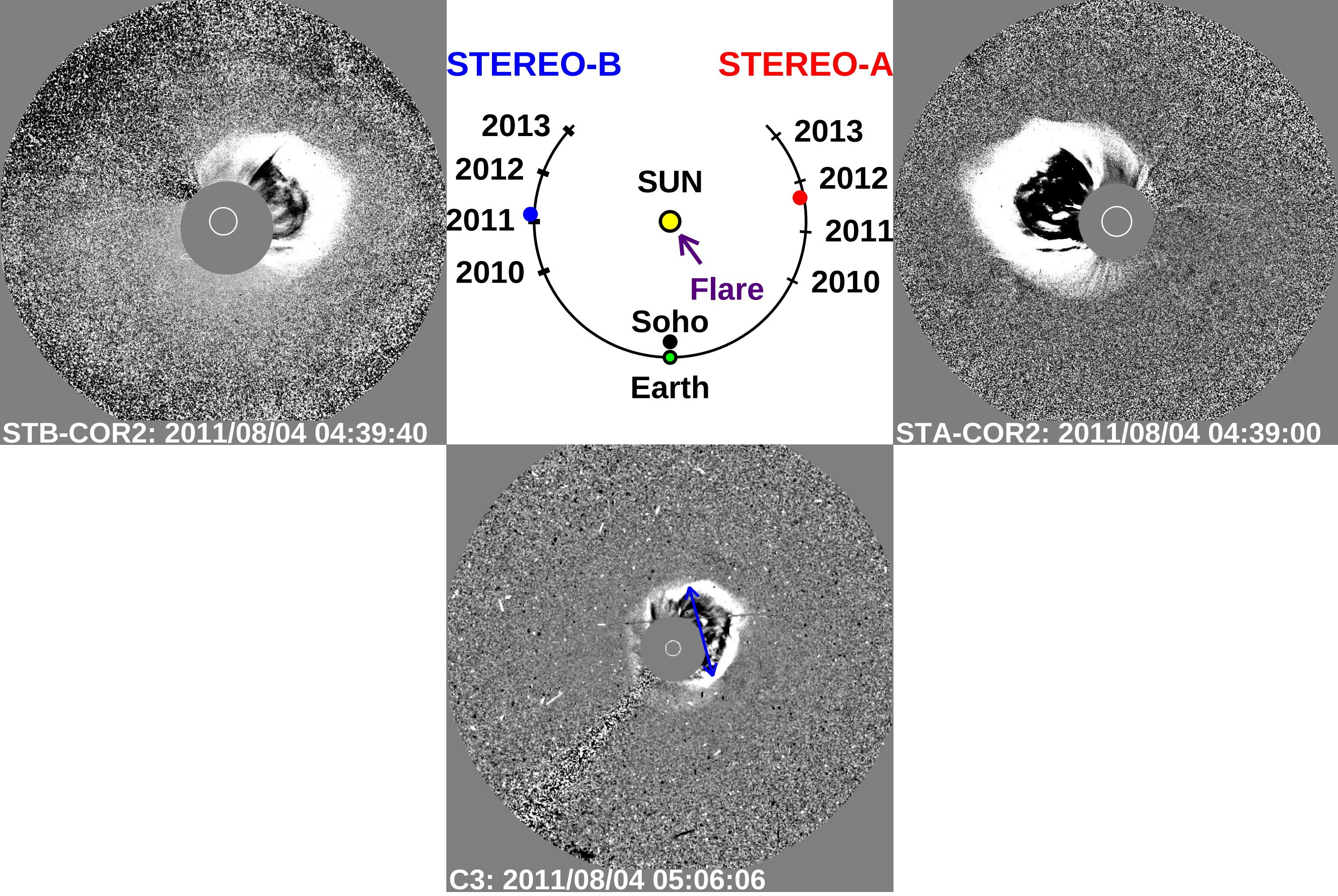
STEREO-B
STEREO-A
2013
2012
2011
2010
2013
2012
2011
2010
SUN
Flare
Soho
Earth
STB-COR2: 2011/08/04 04:39:40
STA-COR2: 2011/08/04 04:39:00
C3: 2011/08/04 05:06:06

(a) Full Ice-Cream Cone **(b) Shallow Cone** **(c) Flat Cone**

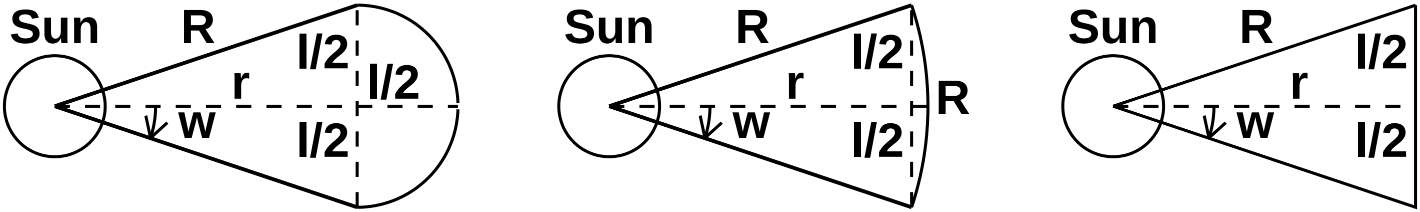

$V_{rad} = 1/2(1 + \cot(w))V_{exp}$

$V_{rad} = 1/2 \operatorname{cosec}(w)\, V_{exp}$

$V_{rad} = 1/2 \cot(w)\, V_{exp}$

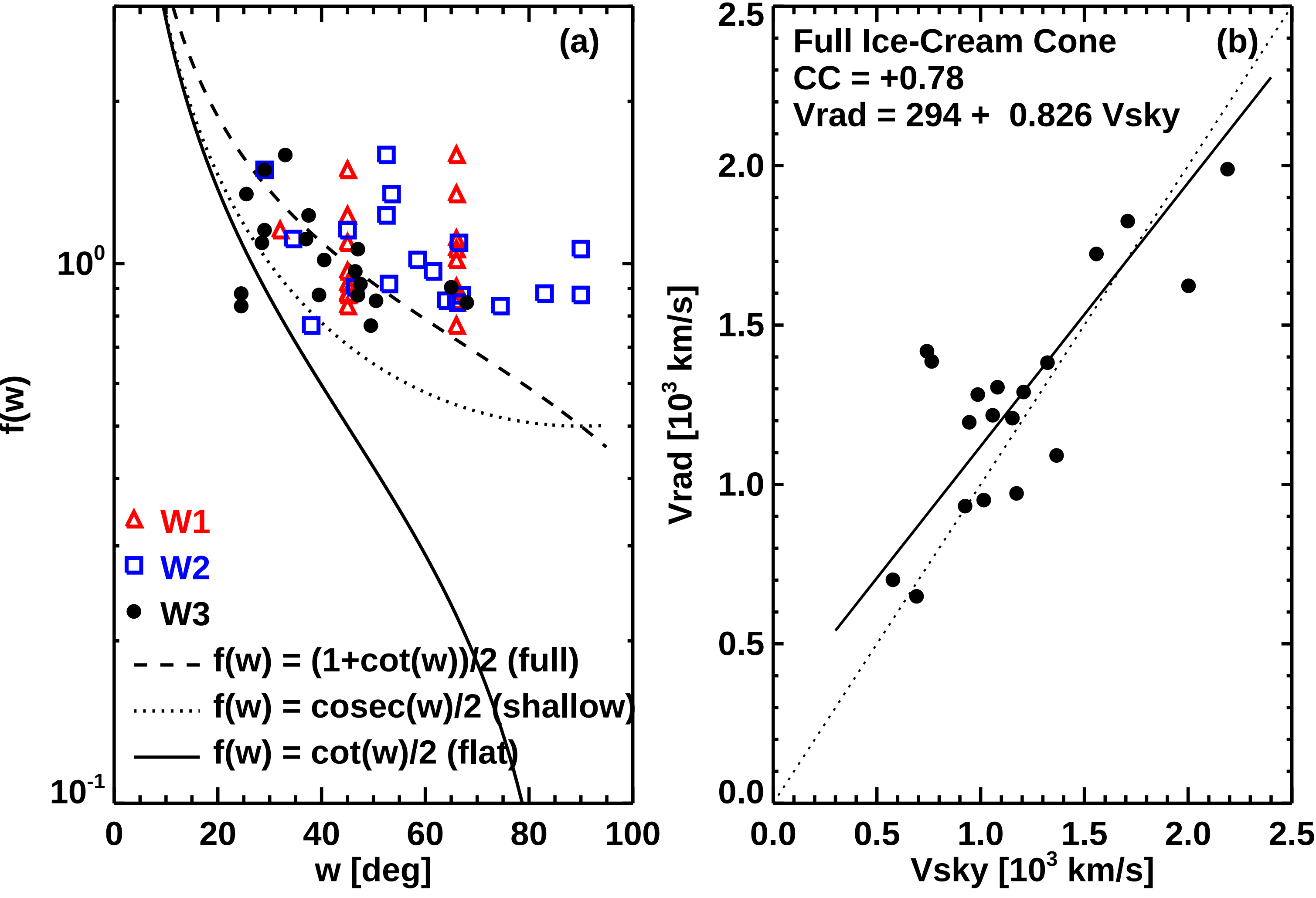

(a)
f(w)
w [deg]
W1
W2
W3
f(w) = (1+cot(w))/2 (full)
f(w) = cosec(w)/2 (shallow)
f(w) = cot(w)/2 (flat)
(b)
Full Ice-Cream Cone
CC = +0.78
Vrad = 294 + 0.826 Vsky
Vrad [10^3 km/s]
Vsky [10^3 km/s]

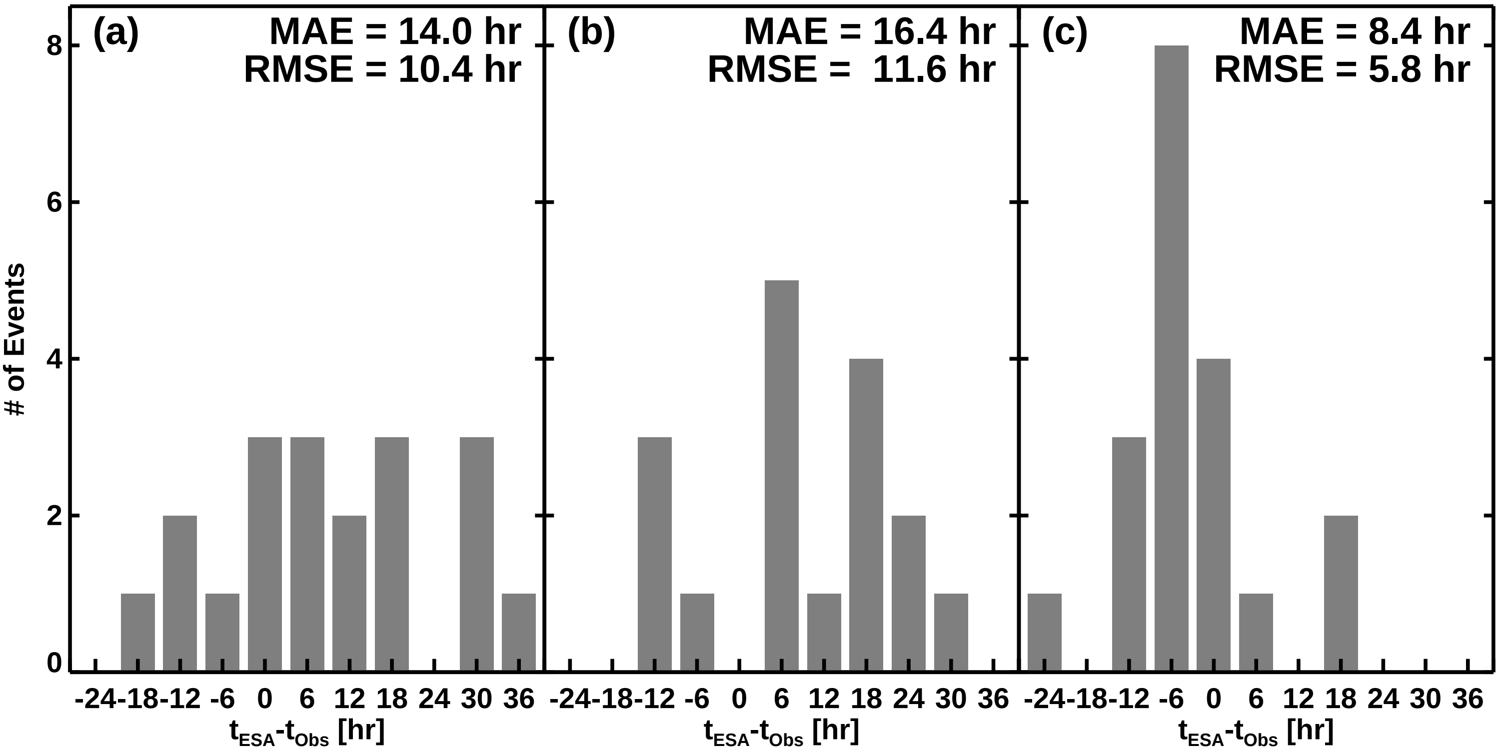
(a)
MAE = 14.0 hr
RMSE = 10.4 hr
(b)
MAE = 16.4 hr
RMSE = 11.6 hr
(c)
MAE = 8.4 hr
RMSE = 5.8 hr
# of Events
0
2
4
6
8
-24 -18 -12 -6 0 6 12 18 24 30 36
t_{ESA}-t_{Obs} [hr]